Alkali chlorides for the suppression of the interfacial recombination in inverted planar perovskite solar cells

Wei Chen, Yecheng Zhou, Guocong Chen, Yinghui Wu, Bao Tu, Fang-zhou Liu, Li Huang, Alan Man Ching Ng, Aleksandra B. Djurišić, Zhubing He**

W. Chen, G. Chen, Y. Wu, B. Tu, Prof. Z. He
Department of Materials Science and Engineering, Shenzhen Key Laboratory of Full Spectral Solar Electricity Generation (FSSEG), Southern University of Science and Technology, No. 1088, Xueyuan Rd., Shenzhen, 518055, Guangdong, P.R. China.
E-mail: hezb@sustc.edu.cn

W. Chen, Dr. F. Z. Liu, Prof. A. B. Djurišić
Department of Physics, The University of Hong Kong, Pokfulam, Hong Kong SAR
E-mail: dalek@hku.hk

Dr. Y. Zhou, Prof. L. Huang and Prof. A. M. Ng
Department of Physics, Southern University of Science and Technology of China, Shenzhen, China, 518055

Keywords: Halide perovskite, Alkali chlorides, interfacial recombination, Nickel Oxide

In this work, we achieved significant suppression of the interfacial recombination by facile alkali chloride interface modification of the NiOx hole transport layer in inverted planar perovskite solar cells. Experimental and theoretical results reveal the alkali chloride interface modification results in improved ordering of the perovskite films, which in turn reduces defect/trap density, causing reduced interfacial recombination. This leads to a significant improvement in the open circuit voltage from 1.07 eV for pristine NiOx to 1.15 eV for KCl treated NiOx, resulting in a power conversion efficiency aproaching 21%. Furthermore, the suppression of the ion diffusion in the devices was observed, as evidenced by stable photoluminescence under illumination and high PL quantum efficiency with alkali chloride treatment, as opposed to the luminescence enhancement and low PL quantum efficiency observed for perovskite on pristine NiOx. The suppressed ion diffusion is also consistent with improved stability of the devices with KCl-treated NiOx. Thus, we demonstrate that a simple interfacial modification is an effective method to not only suppress interfacial recombination

but also to suppress ion migration in the layers deposited on the modified interface due to improved interface ordering and reduced defect density.

1. Introduction

Perovskite solar cells (PSCs) have been attracting increasing attention in recent years due to their exceptional efficiency and potential for low cost production.[1-6] High performance devices have been reported for a variety of active layer compositions and device architectures (both conventional and inverted). While the major part of the research work on the PSCs is focused on the improvement of the perovskite film composition and quality, there has also been increasing awareness of the importance of interfaces in the PSCs.[7-12] The interfaces affect not only the power conversion efficiency due to interfacial defects, energy level alignment and charge distribution, but also the device stability due to ion diffusion and resulting chemical reactions and degradation.[13] Consequently, a variety of interface modifications for different interfaces in the devices has been proposed in order to achieve better energy alignment, passivate the traps, improve the morphology of the active layer, reduce recombination, charge accumulation and hysteresis, as well as improve stability.[8, 14-20] Various organic[8, 15, 20] and inorganic[17, 21] materials for interface modifications and/or interfacial layers have been proposed for both electron transport layer (ETL) and hole transport layer (HTL).

However, the majority of the reported work focused on interface modifications of devices in conventional architecture, while considerably less work has been done on charge transport layer interfaces in inverted devices.[7, 8, 14] Though there have been reports on NiO_x doping with various elements to achieve improved energy band structure alignment across the interface,[7, 18, 22, 23] the methods of modifying the interface of NiO-based HTL have been scarce.[14, 24] For example, it has been previously reported that a monolayer of 5-aminovaleric acid (5-AVA) molecules improved the performance of PSCs with a NiMgLiO HTL.[14, 22, 25] Both efficiency and stability were improved with this modification, which has resulted in

more efficient charge collection and improved perovskite film quality.[14] However, more comprehensive investigations into different surface-modifying agents and physical principles responsible for the observed performance enhancements have been lacking.

Since the NiO-based inverted PSCs are highly promising for flexible devices due to their negligible hysteresis and low processing temperatures compatible with flexible substrates,[26, 27] it is worthwhile to perform a comprehensive investigation of NiO_x/perovskite interface and the methods to improve this interface. Alkali halides (NaCl, KCl, CsBr, KI) have been previously used as additives in processing the perovskite films[28],[29] and as passivation layers on ETL.[17, 21] In addition, Cl-capping was demonstrated to passivate defects in TiO_2 nanocrystal-based ETL.[30] Therefore, we explored the effect of facile alkali halide (NaCl, KCl) interfacial passivation of the NiO_x HTL on the performance of inverted PSCs. Comprehensive theoretical and experimental investigation has been conducted to investigate the effect of the alkali chloride layer on the interface quality, defect density, and recombination losses, and consequently its effect on the efficiency and stability of the inverted PSCs. We demonstrate that the KCl interfacial passivation results in high efficiency devices with PCE of 20.96% with a high open circuit voltage V_{oc} of 1.15 eV, which at the same time exhibit significant improvement in stability compared to pristine NiO_x.

2. Results and Discussion

Figure 1a shows the schematic diagram of the inverted planar perovskite solar cells, while the cross-sectional scanning electron microscopy (SEM) image and illustration of structural details at the NiO_x/NaCl/perovskite interface are shown in **Figure 1b** and **Figure 1c**, respectively (see experimental section for more details of device construction). Cesium (Cs^+), $HC(NH)_2^+$ and $CH_3NH_3^+$ (CsFAMA) ternary cations perovskite precursors were employed to fabricate the high quality perovskite films, and [6,6]-thienyl C_{61} butyric acid methyl ester ($PC_{61}BM$) were used as ETLs. From the photovoltaic performance of the devices, illustrated

in **Figure 1d-f** and **Table 1**, as well as **Figure S1** and **Figure S2** in supporting information, we can observe that alkali chloride (MCl, where M denotes Na or K) modification of the NiO_x surface results in obvious improvement of photovoltaic performance in both reverse and forward scan directions, as well as stabilized short circuit current density and efficiency. All the devices exhibit very small hysteresis, as expected for the inverted planar perovskites with NiO_x HTL and $PC_{61}BM$ ETL.[18, 31, 32] In addition, there is excellent agreement (less than 3% mismatch) between the short circuit current density values determined experimentally and estimated from the measured external quantum efficiency (EQE) spectra. From **Figure 1d** and **Table 1**, we can clearly observe that the differences in the short circuit current density (J_{sc}) and fill factor (FF) for the devices with pristine and modified NiO_x HTLs are very small. The main contribution towards efficiency increase is a significant improvement in the open circuit voltage (V_{oc}) from 1.07 V for pristine NiO_x-based devices to 1.15V for KCl modified NiO_x-based device. This indicates that changes happen at the NiO_x/MCl/perovskite interface, and in the following we will investigate the mechanisms responsible for the increase in V_{oc} in detail.

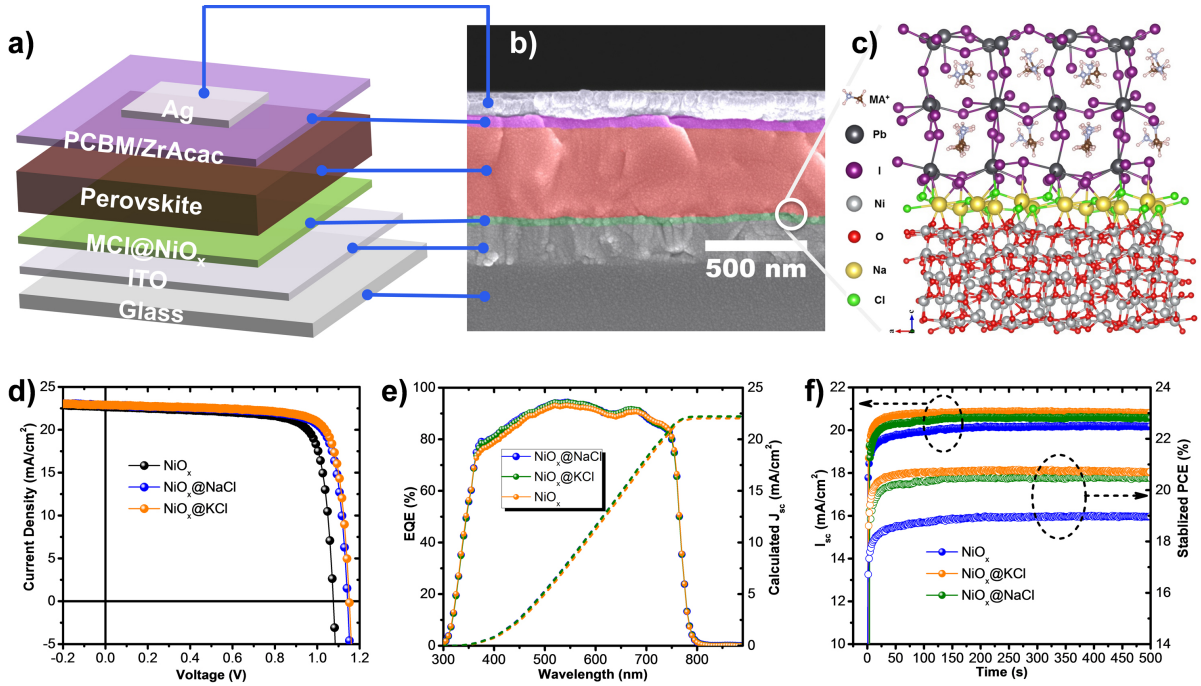

Figure 1. Schematic diagram of device structure of perovskite solar cells (PSCs) used in this work. Pristine or alkali chlorides (MCl) modified NiO_x were used as HTLs; b) Cross section SEM image of a typical PSCs with CsFAMA perovskite and NaCl modified NiO_x HTLs; c) A

supercell illustrating the structural details in perovskite/NaCl/NiO_x HTL interface; d) Current-Voltage characteristics of the optimal CsFAMA PSCs with pristine or alkali chlorides (MCl) modified NiO_x HTLs; e) EQE spectra of the corresponding PSCs in (d); f) Stabilized PCE of the corresponding PSCs in (d).

Table1. Summary of photovoltaic parameters for the inverted PSCs with CsFAMA perovskite with pristine and alkali chlorides modified NiO_x HTLs.

Devices	*Scan direction*	*J_{sc} (mA/cm^2)*	*J_{sc} by EQE (mA/cm^2)*	*V_{oc} (V)*	*FF (%)*	*PCE (%)*
NiO_x	Reverse	22.65	22.03	1.07	79.5	19.27
	Forward	22.67		1.07	78.8	19.11
NiO_x@NaCl	Reverse	22.83	22.20	1.14	79.6	20.71
	Forward	22.88		1.14	79.1	20.63
NiO_x@KCl	Reverse	22.89	22.21	1.15	79.5	20.96
	Forward	22.83		1.15	79.3	20.90

The improvement in the performance of the perovskite deposited on different HTL surfaces has been in some cases attributed to the increase in the quality of the perovskite film, as evidenced by increased grain size.[15] However, we have not observed significant changes in the perovskite film morphology (SEM image in **Figure S3**) and crystallinity (XRD patterns in **Figure S4**). Therefore, different reasons are responsible for the observed performance improvement upon alkali halide surface modification. From the XRD patterns, we can also observe that all perovskite films exhibit good crystallinity, and that there is a presence of some excess PbI_2. The excess PbI_2 was previously proposed to contribute towards high performance[33] and its presence is consistent with obtained high efficiency devices obtained in our work.

To further investigate the interface modification, we have performed scanning transmission electron microscopy (STEM) imaging, Energy-dispersive X-ray (EDX) mapping, X-ray photoelectron spectroscopy (XPS) measurements and Time-of-Flight Secondary Ion Mass Spectrometry (ToF-SIMS) measurements. Obtained results are shown in **Figure 2** and **Figure S5**. Each layer in the device including NiO_x HTLs, perovskite active layers and PCBM ETLs as well as electrodes can be clearly distinguished from the STEM and EDX mapping, indicating the devices are well fabricated, which is consistent with the excellent device performance. We can also observe clear proof of the presence of Na or K in the NiO_x

treated by NaCl or KCl. Furthermore, ToF-SIMS results indicated that Na (or K) is present throughout the NiO_x film, indicating the possibility that it diffuses into the NiO_x film during the deposition procedure, possibly through grain boundaries, while low level of Na (or K) is detected in the perovskite films, confirming that the diffusion of Na (or K) into perovskite film is small. While we cannot exclude some diffusion of the Na (or K) into the perovskite film, due to the lower presence of alkali metal in the perovskite layer and overall low amount of NaCl (or KCl) introduced, we expect that the major effect of alkali chloride is on the NiO_x layer and NiO_x/perovskite interface, rather than perovskite film doping. Consistent with EDX and TOF-SIMS, in the XPS spectra we can observe Cl and Na(K) peaks in the NaCl (KCl) treated films. The Ni $2p_{3/2}$ spectra exhibit typical characteristic Ni peaks in all cases, with the lowest energy peak at ~853.8 eV corresponding to Ni^{2+} and the second lower intensity peak at ~855.4 eV corresponding to Ni^{3+} due to nickel vacancies or nickel hydroxides or nickel oxyhydroxies.[18, 34] O 1s spectra also exhibit two characteristic peaks expected in NiO_x films, and the O_2/O_1 ratio is slightly higher in pristine NiO_x samples, which could occur either due to the change in nickel vacancy concentrations or due to reduced presence of hydroxide or oxyhydroxide at the surface after alkali halide treatment.

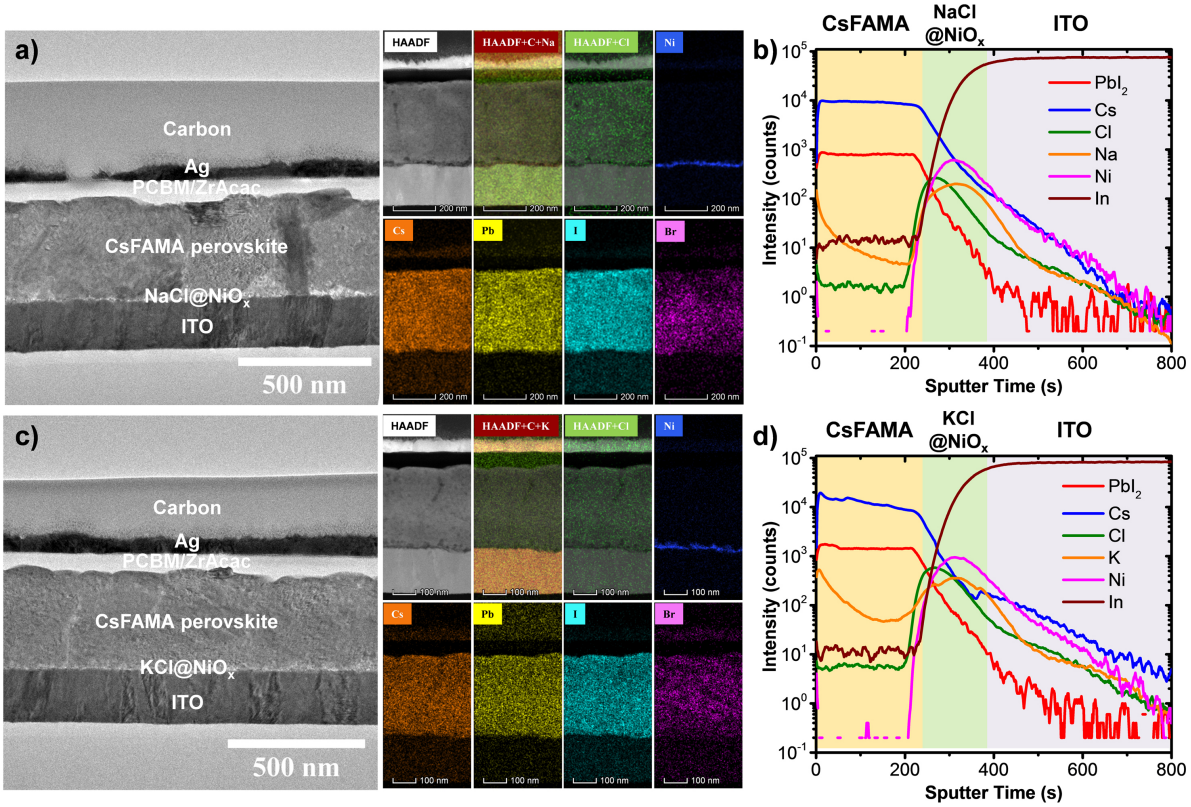

Figure 2. Scanning transmission electron microscopy (STEM) images and the corresponding high resolution EDX mapping of the lateral structure of PSCs with NaCl (a) and KCl (c) modified NiO_x HTLs; TOF-SIMS profiles for the CsFAMA perovskite on NaCl (b) and KCl (d) modified NiO_x HTLs.

The reduced presence of adsorbed hydroxyl groups on the surface could indicate a better quality surface with fewer defects which can serve as adsorption sites for hydroxyl groups. In addition, the distribution of defects in the perovskite film would be affected by the condition of the metal oxide surface, for example uncoordinated metal atoms would serve as acceptor centers and cause preferential formation of anionic defects (organic cation vacancy, I interstitial) near the interface.[35, 36] Obviously, surface modifications have potential to change the initial defect distribution. Consequently, theoretical calculations were performed to obtain more information on how the alkali halide (NaCl or KCl) treatment affects the surface of NiO_x. *Ab initio* molecular dynamics of NiO_x-perovskite and NiO_x-NaCl-perovskite interfaces were performed. The interface was designed by a two layer 2×2 perovskite (001) surface with lattice constant of 12.72 Å× 12.76 Å and a 5 layer of 3 ×3 NiO (001) surface with lattice constant of 12.61 Å× 12.61 Å (Figure S6). Obtained results are shown in **Figure 3**, as well as

Figure S7 and **Figure S8**. Interface strain is 6%. Without a NaCl buffer layer, surface structure re-construction happens (as shown in **Figure 3a**). To our surprise, the perovskite crystal structure in the NiO/perovskite interface with NaCl layer (**Figure 3b**) is much more ordered than the pristine one. This result suggests that the NaCl buffer layer helps to form an ordered interface between NiO and perovskite, which could reduce the defect formation and density of the perovskite surface. Defects which could contribute to the deep levels in the perovskite are antisites I_{Pb}, I_{MA}, Pb_I, Pb_{MA}, iodine vacancy V_I and lead interstitial Pb_i.[36, 37] Among these defects, it was proposed that under certain conditions formation energy of acceptor defect I_{MA} and donor defects Pb_I and V_I can be sufficiently low for these defects to be present at significant concentrations. It has also been proposed that two typical surface defects are Pb_I antisite on PbI_2 terminated surfaces and Pb cluster on MAI-terminated surfaces.[35] Since our films contain excess PbI_2, we examined the Pb_I antisite defect in our calculations, although it should be noted that this defect may have a large formation energy according to some calculations.[38] We built a model with a Pb_I antisite defect, and found that the antisite Pb_I defect recovered by itself after 3 ps molecular dynamics. This suggests that the anti-site Pb-I defect is not stable. Therefore, the observed improvement cannot be attributed to the elimination of Pb-I antisites. Thus, we argue that the halide elements indeed heal the interface contact, but this healing is probably caused by the interface structure ordering induced by NaCl.

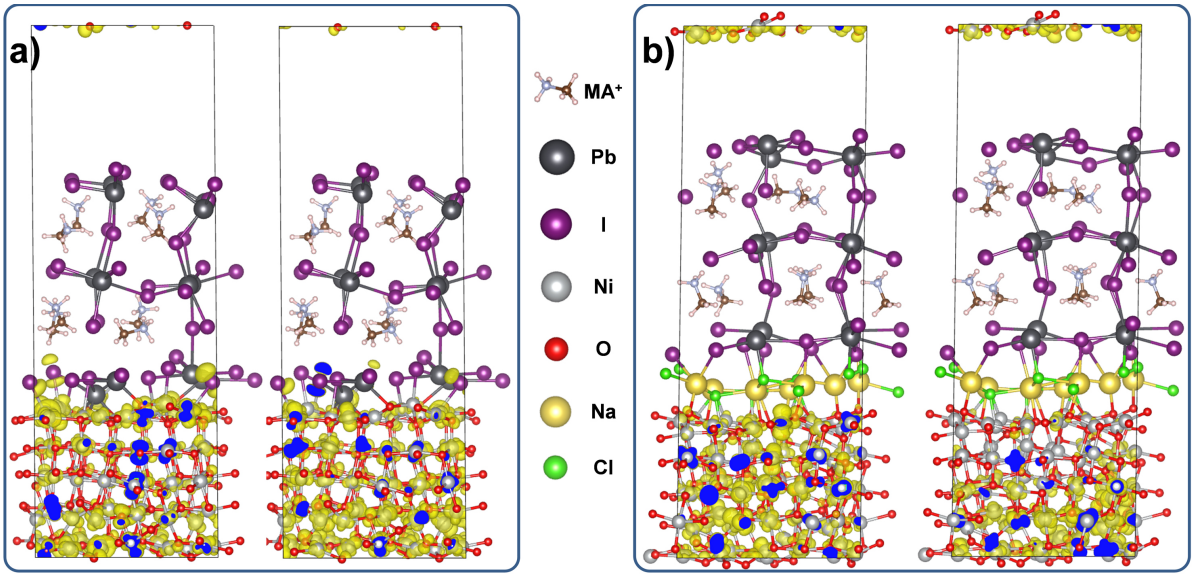

Figure 3. Ab initio molecular dynamics (MD) of NiO-perovskite (a) and NiO-NaCl-perovskite (b) interfaces. For simplifying the calculation, $MAPbI_3$ perovskite supercell was used for MD simulation.

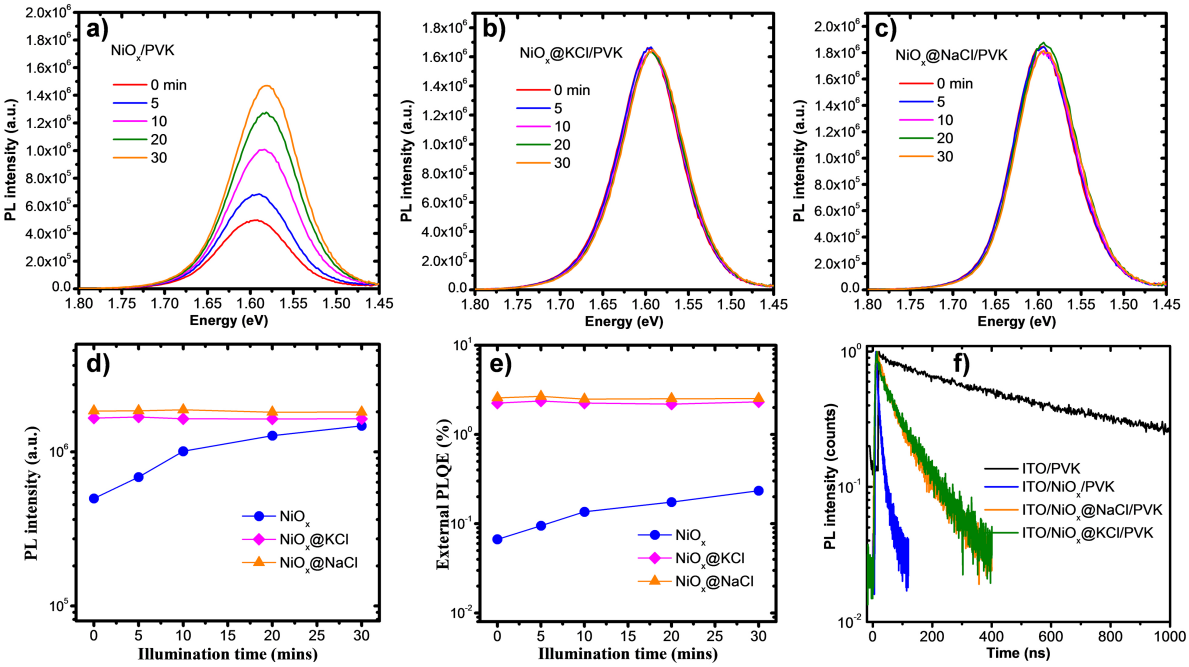

Figure4. Steady photoluminescence (PL) spectra of CsFAMA perovskite films on NiO_x (a), NiO_x@KCl (b) and NiO_x@NaCl (c) HTLs; d) PL peak intensities of the corresponding CsFAMA perovskite films as function of aging time. The excitation wavelength is 550 nm and film were illuminated with white LED lamp with intensity of ~ 50mW/cm^2; e) External PL quantum efficiency (QE) of the corresponding CsFAMA perovskite films; f) PL decay dynamics of the corresponding CsFAMA perovskite films. Pulsed laser of 400 nm is used for TRPL measurement.

Table 2. Summary of the PL lifetime parameters from fitting curves of the PL decay measurements.

Samples	B_1 (%)	τ_1[ns]	B_2 (%)	τ_2[ns]	Weighted average τ [ns]

ITO/PVK	23.1	125.2	76.9	784.8	754.6
ITO/NiO_x/PVK	4.4	2.6	95.6	6.9	6.8
ITO/NiO_x@NaCl/PVK	44.6	12.1	55.4	96.8	89.1
ITO/NiO_x@KCl/PVK	47.7	13.6	52.3	105.5	95.8

To obtain further information about the effect of alkali chloride interface modification, photoluminescence spectroscopy investigations were conducted, and the obtained results are shown in **Figure 4**. Time resolved photoluminescence (TRPL) spectra show in **Figure 4f** can be fitted by a bi-exponential decay,[9, 39] and the obtained parameters are shown in **Table 2.** A reduction in photoluminescence (PL) intensity and PL decay time indicates more efficient electron transfer from the perovskite to the HTL.[9, 34] From the obtained data, it appears that the charge injection is less efficient after the interface modification by alkali chlorides, as evidenced by longer PL decay times and higher intensities of the PL and external PL quantum efficiency (PLQE) (**Figure 4d and e**). However, we can also observe a significant difference in the behavior of perovskite films on pristine NiO_x and alkali chloride treated NiO_x, namely the dependence of PL intensity on the illumination time (**Figure 4a-d**). The changes of the PL intensity over time (increase or decrease) of illumination have been previously observed in halide perovskites.[29, 40-42] The increase of the PL with illumination time in the perovskite films has been attributed to the I_i defects[40, 41] and iodide migration.[42] Since the ion migration is affected by the presence of native defects, it is expected that the films prepared on alkali halide modified surfaces would exhibit lower rates of ion migration. It should also be pointed out that the presence of interstitial alkali cations in perovskites can suppress the ion migration.[43] Although Na and K are mainly located within NiO_x and at the NiO_x perovskite interface, there is a low presence of Na or K in the perovskite films and therefore the possible effect of Na_i (K_i) cannot be entirely excluded. Thus, the PL intensity dependence on time indicates that there are either more defects or more ion accumulation at HTL/perovskite interface with pristine NiO_x. However, the TRPL data indicate increased PL decay time for

alkali halide modified surfaces, which can occur either due to increased quality of the perovskite (reduced nonradiative recombination)[44, 45] with similar efficiency of charge transfer, or less efficient charge transfer to the HTL. To examine the charge collection, we performed conductive AFM scans of the HTL films (**Figure S9**), and we found similar levels of current, with small increase for KCl-modified sample compared to the other two. Similar currents in the samples indicate that alkali chloride treatment does not result in significant doping or increase in the conductivity of HTL. From the UPS measurements (**Figure S10**), we can observe a slight increase in the work function of the alkali chloride treated samples. These shifts in the energy level could affect charge collection, with an increase in work function leading to better charge collection.[46] This would indeed be consistent with an observed small increase in J_{sc}, and thus the observed increase in the TRPL decay time and enhanced PLQE could occur due to reduced nonradiative recombination. Since an interface modification of a PTAA HTL was shown to lead to both increased V_{oc} and increased TRPL decay time due to suppressed interfacial recombination[45] in agreement with our results for KCl@NiO_x, the suppression of interfacial recombination by increased ordering and consequently reduced defect formation in the perovskite layer could explain the observed behavior.

To further investigate the interfacial traps and recombination, comprehensive characterization was performed using admittance spectroscopy, photovoltage transients, I-V curve measurements in the dark and under different illumination intensities. Since films and devices with KCl and NaCl-modified NiO_x exhibit similar behavior, but KCl modification results in better device performance, further study was conducted on devices with KCl@NiO_x. Admittance spectroscopy is an effective method to analyze the density of trap states (DOS) in thin-film photovoltaics.[47-49] The distribution of the trap state density can be described as $DOS(E_\omega) = -\frac{V_{bi}}{qW}\frac{dC}{d\omega}\frac{\omega}{KT}$, where V_{bi}, W, C, ω, K, q and T are built-in potential, depletion

width, capacitance, angular frequency, Boltzmann constant, elementary charge and temperature, respectively.[47-49] V_{bi} can be obtained from the $1/C^2$–V Mott-Schottky plots shown in **Figure 5a**, where V_{bi} is given by the intersection on the bias axis.[47-49] The obtained trap density shown in **Figure 5b** is in the range expected for a polycrystalline halide perovskite film.[35] We do not observe any disappearance of the trap states or change in the position of the trap states with alkali chloride surface modification, but we observe a reduction in the trap state density for both trap states with depths ~0.35-0.47 eV and 0.5-0.6 eV. It was previously proposed that traps in the region 0.40-0.52 eV correspond to the defects at film surface, while the shallower traps in the region 0.35-0.40 eV correspond to traps in grain boundaries.[35] The reduction in the trap density both on the surface and in the grain boundaries indicates that the interface quality has significant influence on the formation of defects in the perovskite film. The reduction in the trap density is also in agreement with the reduction in the trap-filled limit voltage (V_{TFL}) which is directly proportional to the trap density,[30] as shown in the dark I-V characteristics of hole-only devices (**Figure 6a**).

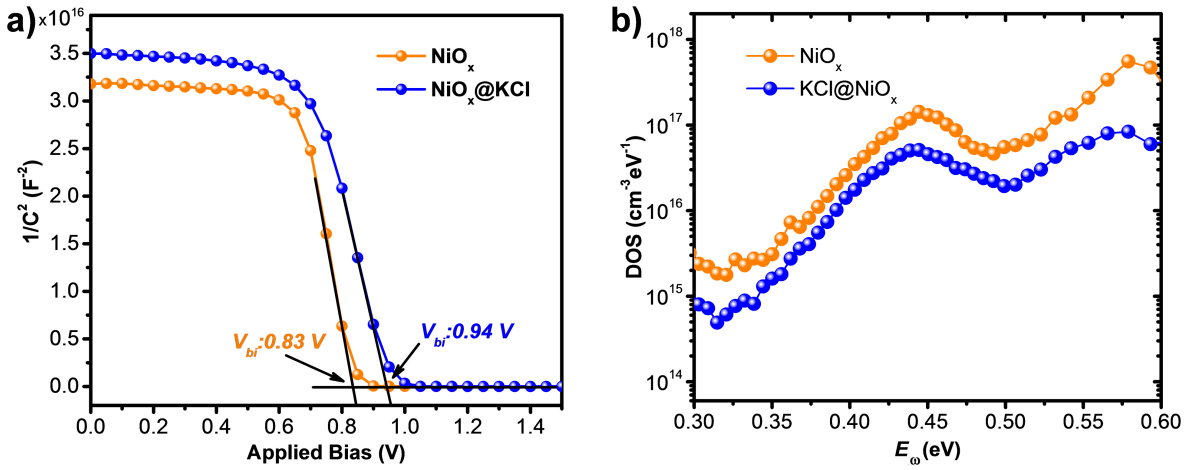

Figure 5. (a) Mott–Schottky plots for the CsFAMA perovskite PSCs with pristine and KCl modified NiO_x HTLs at 10 kHz. (b) Trap density of states (DOS) spectra for CsFAMA perovskite PSCs with pristine and KCl modified NiO_x HTLs. All measurement was measured under ambient environment (~23 ^oC, ~37% humidity) under dark. and E_ω is the energy demarcation determined by the applied angular frequency. E_ω denotes the energy demarcation determined by the applied angular frequency $E_\omega = kt\, ln\frac{\omega_0}{\omega}$.

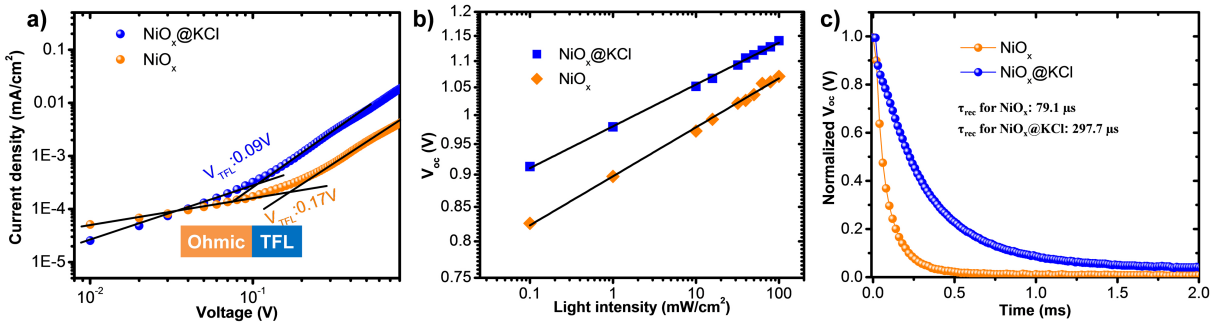

Figure6. a) Dark I-V characteristics of the hole only devices with structure of ITO/NiO_x or NiO_x@KCl/CsFAMA perovskite/Spiro-MeOTAD/Au; b) Open circuit voltage (V_{oc}) evaluation of the PSCs with different HTLs under various illumination intensity; c) V_{oc} decay dynamics of the PSCs with different HTLs.

To further characterize the devices, we investigated the dependence of the photovoltaic parameters on the illumination power. J-V curves under different light intensities are shown in **Figure S11**, while the dependence of the J_{sc} on the light intensities is shown in in **Figure S12** and the dependence of the V_{oc} on the light intensities are shown in **Figure 6b**, while V_{oc} transient measurement is shown in **Figure 6c**. We can observe significantly slower photovoltage decay for KCl@NiO_x, which is consistent with reduced recombination losses.[30, 39] The increase in the charge recombination lifetime has been attributed to a more favorable energy level alignment and improved electron blocking (carrier selectivity)[15] or reduced charge carrier accumulation due to more efficient charge extraction.[22] Reduced interfacial recombination is also consistent with reduced diode ideality factor deduced from V_{oc} dependence on the light intensity,[30] from 1.45 to 1.23 for NiO_x and KCl modified NiO_x, respectively. Lower ideality factor indicates lower trap-assisted Shockley-Read-Hall monomolecular recombination,[46, 50] which is consistent with the lower trap densities for perovskite on KCl modified NiO_x. Reduced recombination is also consistent with a significant increase in the open circuit voltage.[45] While the relationship between V_{oc} and recombination can be complex, [51] in the absence of significant changes of grain size and hysteresis/charge accumulation, it would be expected that reduced recombination would result in increased V_{oc}.

To examine whether interface passivation by alkali chloride is generally applicable to perovskite materials with different compositions, cells with $MAPbI_3$ active layers were prepared and characterized. Obtained results are summarized in **Table S1** and **Figure S13**. It can be observed that in this case even more significant improvement in the performance is obtained compared to CsFAMA-based active layers. Finally, we examined the stability of PSCs with CsFAMA-based active layers for pristine and KCl modified NiO_x and the obtained results are shown in **Figure 7** and **Table 3**. Significant improvement in device stability is obtained for KCl modification. As we can see, the KCl modified devices maintained over 95% of initial performance after 150 days storage at nitrogen filled dry box, while the efficiency of the pristine NiO_x based devices was reduced to ~85% of the initial one. PCE of best tested pristine and KCl modified device decreased from to 19.10% and 20.57% to 16.83 % and 19.52% after 150 days (**Figure 7e** and **f**), respectively. It has been previously shown that the defect passivation can result in significant improvement of the device stability and lifetime.[35, 36] Alkali chloride interface modification of the ETLs has also been shown to results in the improvement in PSC stability.[17, 21] It is well recognized that the device degradation starts with the interfacial degradation, which would induce the dramatic increase of charge recombination and charge transfer losses, resulting in the decrease of the device performance.[52] The obtained improvement in the device stability in our work is consistent with previous results and it can likely be attributed to the interfacial defect passivation, suppressed interfacial recombination and the reduction of trap density in the perovskite layer via alkali chloride modification of the HTLs. Lower stability of devices with pristine NiO_x is also consistent with the increase of PL intensity over time, indicating significant presence of defects facilitating ion diffusion. As a result, our work presents a facile and simple strategy to suppress interfacial losses in perovskite solar cells and pave a way for improving the device efficiency and stability.

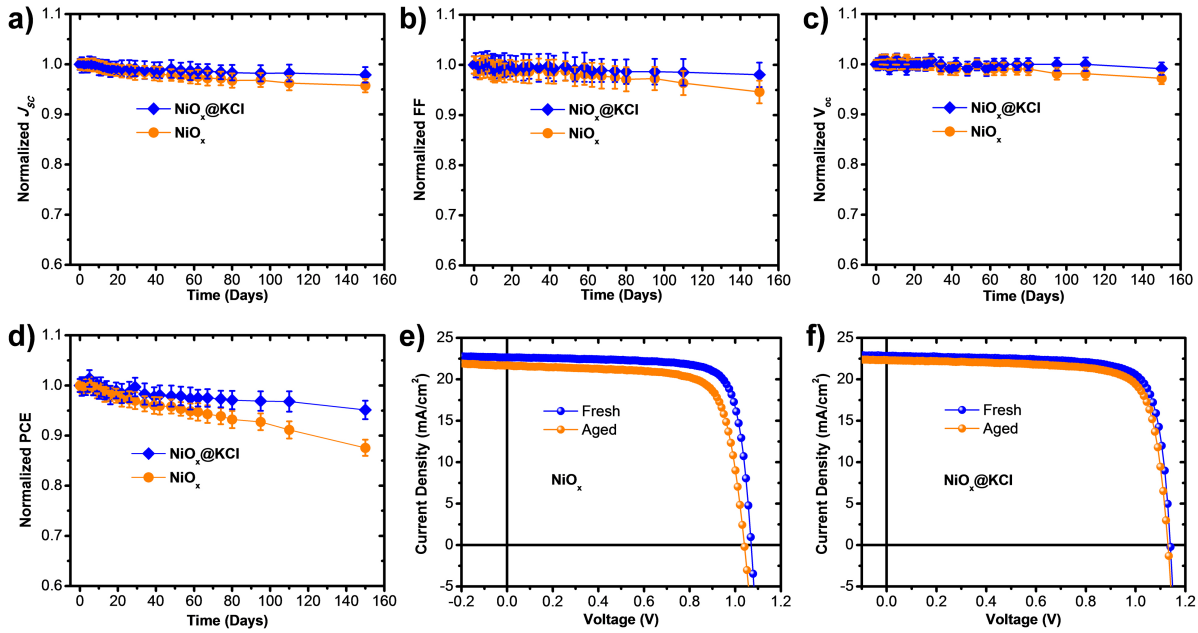

Figure7. Normalized photovoltaic parameters of (a) J_{sc}, (b) FF, (c) V_{oc} and (d) PCE for the CsFAMA perovskite PSCs with pristine and KCl modified NiO_x HTLs as function of aging time, averaged values are obtained from 6 tested devices; e) and f) I-V curves of the best cells before and after aging of 150 days. The devices were encapsulated and stored at inert environment under dark during aging test.

Table 3 Summary of photovoltaic parameters for the tested best PSCs with different HTLs before and after 150 days aging.

Devices		***J_{sc} (mA/cm^2)***	***V_{oc} (V)***	***FF (%)***	***PCE (%)***
NiO_x	Fresh	22.64	1.06	78.8	18.92
	After aging	21.69	1.03	74.6	16.67
NiO_x@KCl	Fresh	22.83	1.14	79.5	20.57
	After aging	22.31	1.13	77.2	19.46

3. Conclusion

In summary, we investigated the use of alkali chloride (NaCl, KCl) interface modification in inverted planar PSCs. We found that the alkali chloride interfacial layer resulted in improved ordering of the perovskite layer deposited on modified NiO_x, which leads to reduced defect density in the films and substantial reduction in the interfacial recombination. The performance improvements with surface modification are applicable both to MA and CsFAMA-based perovskite active layers. The best performing devices with KCl@NiO_x HTL and CsFAMA active layer exibit open circuit voltage as high as 1.15 V, leading to the PCE of 20.96%. The alkali halide interface modification resulted not only in improved efficiency via

suppressed interfacial recombination, but also to improved device stability which we attribute to the improved order and reduced defect density in the perovskite layer.

4. Experimental Section

Materials: All anhydrous solvents including N,N-dimethylformamide (DMF, 99.8%), dimethyl sulfoxide (DMSO, 99.8%), isopropanol (IPA, 99.8%), chlorobenzene (CB, 99.8%) and all other solvents were purchased from Acros Organics. Sodium chloride (NaCl, 99.999%), potassium chloride (KCl, 99.999%) and cesium iodide (CsI, 99.999 %) were purchased from Sigma-Aldrich. Zirconium (IV) acetylacetonate (ZrAcac, 97%), Nickel(II) nitrate hexahydrate (98%), Lead (II) iodide (PbI_2) and lead (II) bromide ($PbBr_2$) were purchased from TCI. Methylammonium bromide (MABr), formamidinium Iodide (FAI) were purchased from GreatCell Solar Ltd (Australia). PCBM (99.5%) were obtained from Lumtec (Taiwan, China). All materials above were used as received.

Device Fabrication: ITO glass was cleaned by sequentially washing with detergent, deionized (DI) water, acetone, and isopropanol (IPA), followed by exposure to UV ozone for 15 min. immediately before use. NiO_x HTLs were prepared on the clean ITO substrates by spin coating fresh prepared NiO_x nanoparticle inks according to our previously reported method.[25, 53] The alkali chlorides (KCl and NaCl, 5mg/ml in DI water) were then spin coated on NiO_x HTLs (5000 rpm, 60s). The films were annealed at 120 ºC for 15 min in air. After cooling down, HTLs were transferred to N_2 glove box for next procedure. Both $MAPbI_3$ perovskite and CsFAMA mixed perovskite films were deposited through antisolvent assisted one-step procedure according to our previously reported methods.[25, 46] For $MAPbI_3$ perovskite film preparation, precursor solution consisting of stoichiometric PbI_2 and MAI (1.3 M) in a mixture of DMF and DMSO (4:1 v/v) was filtered using 0.45 µm PTFE syringe filter and coated onto the corresponding HTLs coated substrates with speed of 1000 rpm for 10 s and 5000 rpm for 25 s. During the last 10 s of the spinning process, the substrate was treated by drop-casting chlorobenzene solvent. The substrates were then annealed on a hot plate at 50

°C for 1 min and 100 °C for 15 min. For CsFAMA perovskite film, precursor solution was made by mixing PbI_2, $PbBr_2$, FAI and MAI in DMF/DMSO (v/v 4/1). The mole concentration was kept at 1.3 M with 0.1 M PbI_2 excess. The I/Br and FA/MA mole ratio were maintained at 0.85/0.15. After stirring 1 hour, 35 µl of CsI (2 M in DMSO) was added into the precursor solution and stirred another 1 hour at 65 °C. The CsFAMA perovskite films were prepared by spin coating the precursor solution (4000 rpm, 35s). In the last 25s of the procedure, film were quickly treated with 300 µl CB and annealed at 100 °C for 60 min. PCBM (2 wt% in CB) was subsequently spin coated with on top of perovskite (1000 rpm, 30s), and annealed at 100 ºC for 30 min. After 5 min cooling of PCBM films, ZrAcac (0.1wt% in IPA) was deposited with 5000 rpm spinning speed. Finally, Ag back electrode was deposited by thermal evaporation. The active area was 0.1 cm^2.

Characterization: I–V measurements were carried out using a Keithley 2400 sourcemeter in ambient environment of 27 ºC and ~55% RH. Illumination was provided by an Oriel Sol3A solar simulator with AM1.5G spectrum and light intensity of 100 mW/cm^2 was calibrated using a KG-5 Si diode. The devices were measured both in reverse scan (1.2 V→-0.2 V, step 0.01 V) and forward scan (-0.2 V→1.2 V, step 0.01 V) with 10 ms delay time. EQE measurements were performed with an Enli Tech (Taiwan) EQE measurement system, and the light intensity was calibrated with a standard single-crystal Si photovoltaic cell. All AFM-based experiments were measured in ambient condition (25 ºC and 38% RH) with Atomic Force Microscope (AFM) (MFP-3D-BIO, Asylum Research, USA). Pt/Ir coated silicon tips (Econo-SCM-PIC) with a spring constant of k ~ 0.4-0.7 N/m, a resonance frequency at ~ 9-17 KHz were used in c-AFM imaging. UPS and XPS measurements were performed on an ESCALAB 250Xi, Thermo Fisher (by using Al Kα x-ray source) under high vacuum (10^{-9} mbar). For work function measurement with UPS, -10 V bias was applied and Au was used as reference. The XPS spectra were calibrated by the binding energy of C 1s. Top-view

morphology was analyzed by TESCAN MIRA3, cross-section morphology. A FEI Helios Nanolab 600i dual beam focus ion beam/field emission gun-scanning electron microscope (FIB/FEGSEM) was used to prepare cross-section for STEM imaging and analysis. FEI Talos transmission electron microscope (TEM) with Super-X EDX was employed to acquire the STEM-EDX data with high-angle annular dark field (STEM-HAADF) mode. Depth profiling data were obtained with ToF-SIMS 5 system from ION-TOF. The X-ray diffraction patterns were taken on BRUKER ECO D8 series. PL and time resolved PL spectra were carried out by Spectrofluorometer (FS5, Edinburgh instruments). Xenon lamp and 405 nm pulsed laser were used as excitation sources for the PL and TRPL measurement, respectively. External photoluminescence quantum efficiency (QE) measurements were taken by mounting perovskite films in an integrating sphere. The admittance spectroscopy was measured by a Zahner IM6e electrochemical station (Zahner, Germany) in ambient environment of 23 ºC and 37% RH. Transient photovoltage measurement was performed with controlled intensity modulated photo spectroscopy (CIMPS) system provided by Zennium workstation (ZAHNER-elektrik GmbH).

Theoretical calculations: First-principle calculations were performed with the Vienna Ab Initio Simulation Package (VASP). The projector augmented-wave (PAW) method and generalized gradient approximation (GGA) with the exchange-correlation energy functional of Perdew-Burke-Ernzerhof revised for solid was utilized, which have been tested that gave the most correct perovskite lattice constant.[54] Plane waves with a kinetic energy cutoff of 400 eV for basis function sets were employed. All *ab-initio* molecular dynamics were simulated by micro canonical ensemble with a time step of 1fs.

Supporting Information
Supporting Information is available from the Wiley Online Library or from the author.

Acknowledgements
W. Chen and Dr. Y.C. Zhou contributed equally to this work. This work is supported by the National Natural Science Foundation of China (NSFC) (No. 61775091), National Key

Research Project MOST (No. 2016YFA0202400), the Shenzhen Key Laboratory Project (No. ZDSYS201602261933302) and Natural Science Foundation of Shenzhen Innovation Committee (Nos. JCYJ20150529152146471, JCYJ20170818141216288). The authors are grateful for support from the Seed Funding for Strategic Interdisciplinary Research Scheme of the University of Hong Kong and RGC GRF grants 15204515 and 15246816 are also acknowledged. The authors thank the Materials Characterization and Preparation Center (MCPC) and the Pico Center of SUSTech for some characterizations in this work.

Received: ((will be filled in by the editorial staff))
Revised: ((will be filled in by the editorial staff))
Published online: ((will be filled in by the editorial staff))

References

[1] J. P. Correa-Baena, M. Saliba, T. Buonassisi, M. Gratzel, A. Abate, W. Tress, A. Hagfeldt, *Science* **2017**, *358*, 739.

[2] Y. Rong, Y. Hu, A. Mei, H. Tan, M. I. Saidaminov, S. I. Seok, M. D. McGehee, E. H. Sargent, H. Han, *Science* **2018**, *361*, eaat8235.

[3] T. M. Brenner, D. A. Egger, L. Kronik, G. Hodes, D. Cahen, *Nat. Rev. Mater.* **2016**, *1*, 15007.

[4] J. Huang, Y. Yuan, Y. Shao, Y. Yan, *Nat. Rev. Mater.* **2017**, *2*, 17042.

[5] Z. Li, T. R. Klein, D. H. Kim, M. Yang, J. J. Berry, M. F. A. M. van Hest, K. Zhu, *Nat. Rev. Mater.* **2018**, *3*, 18017.

[6] D. Li, J. Shi, Y. Xu, Y. Luo, H. Wu, Q. Meng, *Natl. Sci. Rev.* **2018**, *5*, 559.

[7] P. Da, G. Zheng, *Nano Research* **2017**, *10*, 1471.

[8] W. Deng, X. Liang, P. S. Kubiak, P. J. Cameron, *Adv. Energy Mater.* **2018**, *8*, 1701544.

[9] J. Jiang, Z. Jin, J. Lei, Q. Wang, X. Zhang, J. Zhang, F. Gao, S. Liu, *J. Mater. Chem. A* **2017**, *5*, 9514.

[10] S. J. Park, S. Jeon, I. K. Lee, J. Zhang, H. Jeong, J.-Y. Park, J. Bang, T. K. Ahn, H.-W. Shin, B.-G. Kim, H. J. Park, *J. Mater. Chem. A* **2017**, *5*, 13220.

[11] L. Hu, K. Sun, M. Wang, W. Chen, B. Yang, J. Fu, Z. Xiong, X. Li, X. Tang, Z. Zang, S. Zhang, L. Sun, M. Li, *ACS Appl. Mater. Interfaces* **2017**, *9*, 43902.

[12] K. Chen, Q. Hu, T. Liu, L. Zhao, D. Luo, J. Wu, Y. Zhang, W. Zhang, F. Liu, T. P. Russell, R. Zhu, Q. Gong, *Adv. Mater.* **2016**, *28*, 10718.

[13] Q.-D. Ou, C. Li, Q.-K. Wang, Y.-Q. Li, J.-X. Tang, *Adv. Mater. Interfaces* **2017**, *4*, 1600694.

[14] Y. Zhang, S. Zhang, S. Wu, C. Chen, H. Zhu, Z. Xiong, W. Chen, R. Chen, S. Fang, W. Chen, *Adv. Mater. Interfaces* **2018**, *5*, 1800645.

[15] Q. F. Xue, Y. Bai, M. Y. Liu, R. X. Xia, Z. C. Hu, Z. M. Chen, X. F. Jiang, F. Huang, S. H. Yang, Y. Matsuo, H. L. Yip, Y. Cao, *Adv. Energy Mater.* **2017**, *7*, 1602333.

[16] P.-L. Qin, H.-W. Lei, X.-L. Zheng, Q. Liu, H. Tao, G. Yang, W.-J. Ke, L.-B. Xiong, M.-C. Qin, X.-Z. Zhao, G.-J. Fang, *Adv. Mater. Interfaces* **2016**, *3*, 1500799.

[17] W. Li, W. Zhang, S. Van Reenen, R. J. Sutton, J. Fan, A. A. Haghighirad, M. B. Johnston, L. Wang, H. J. Snaith, *Energy Environ. Sci.* **2016**, *9*, 490.

[18] W. Chen, F. Z. Liu, X. Y. Feng, A. B. Djurisic, W. K. Chan, Z. B. He, *Adv. Energy Mater.* **2017**, *7*, 1700722.

[19] J. M. Marin-Beloqui, L. Lanzetta, E. Palomares, *Chem. Mater.* **2016**, *28*, 207.

[20] S. Hong, J. Lee, H. Kang, G. Kim, S. Kee, J. H. Lee, S. Jung, B. Park, S. Kim, H. Back, K. Yu, K. Lee, *Sci. Adv.* **2018**, *4*, eaat3604.

[21] X. Liu, Y. Zhang, L. Shi, Z. Liu, J. Huang, J. S. Yun, Y. Zeng, A. Pu, K. Sun, Z. Hameiri, J. A. Stride, J. Seidel, M. A. Green, X. Hao, *Adv. Energy Mater.* **2018**, *8*, 1800138.

[22] W. Chen, Y. Wu, Y. Yue, J. Liu, W. Zhang, X. Yang, H. Chen, E. Bi, I. Ashraful, M. Gratzel, L. Han, *Science* **2015**, *350*, 944.

[23] J. Ma, M. Zheng, C. Chen, Z. Zhu, X. Zheng, Z. Chen, Y. Guo, C. Liu, Y. Yan, G. Fang, *Adv. Funct. Mater.* **2018**, *28*, 1804128.

[24] Z. Li, B. H. Jo, S. J. Hwang, T. H. Kim, S. Somasundaram, E. Kamaraj, J. Bang, T. K. Ahn, S. Park, H. J. Park, *Adv. Sci.*, *6*, 1802163.

[25] W. Chen, L. Xu, X. Feng, J. Jie, Z. He, *Adv. Mater.* **2017**, *29*, 1603923.

[26] W. Chen, Y. Wu, J. Fan, A. B. Djurišić, F. Liu, H. W. Tam, A. Ng, C. Surya, W. K. Chan, D. Wang, Z.-B. He, *Adv. Energy Mater.* **2018**, *8*, 1703519.

[27] Z. Liu, J. Chang, Z. Lin, L. Zhou, Z. Yang, D. Chen, C. Zhang, S. F. Liu, Y. Hao, *Adv. Energy Mater.* **2018**, *8*, 1703432.

[28] H. Lee, A. Kim, H.-C. Kwon, W. Yang, Y. Oh, D. Lee, J. Moon, *ACS Appl. Mater. Interfaces* **2016**, *8*, 29419.

[29] M. Abdi-Jalebi, Z. Andaji-Garmaroudi, S. Cacovich, C. Stavrakas, B. Philippe, J. M. Richter, M. Alsari, E. P. Booker, E. M. Hutter, A. J. Pearson, S. Lilliu, T. J. Savenije, H. Rensmo, G. Divitini, C. Ducati, R. H. Friend, S. D. Stranks, *Nature* **2018**, *555*, 497.

[30] H. Tan, A. Jain, O. Voznyy, X. Lan, F. P. García de Arquer, J. Z. Fan, R. Quintero-Bermudez, M. Yuan, B. Zhang, Y. Zhao, F. Fan, P. Li, L. N. Quan, Y. Zhao, Z.-H. Lu, Z. Yang, S. Hoogland, E. H. Sargent, *Science* **2017**, *355*, 722.

[31] Y. Hou, W. Chen, D. Baran, T. Stubhan, N. A. Luechinger, B. Hartmeier, M. Richter, J. Min, S. Chen, C. O. Quiroz, N. Li, H. Zhang, T. Heumueller, G. J. Matt, A. Osvet, K.

Forberich, Z. G. Zhang, Y. Li, B. Winter, P. Schweizer, E. Spiecker, C. J. Brabec, *Adv. Mater.* **2016**, *28*, 5112.

[32] W. Chen, Y. Wu, B. Tu, F. Liu, A. B. Djurišić, Z. He, *Appl. Surf. Sci.* **2018**, *451*, 325.

[33] B.-w. Park, N. Kedem, M. Kulbak, D. Y. Lee, W. S. Yang, N. J. Jeon, J. Seo, G. Kim, K. J. Kim, T. J. Shin, G. Hodes, D. Cahen, S. I. Seok, *Nat. Commun.* **2018**, *9*, 3301.

[34] Z. Zhu, Y. Bai, T. Zhang, Z. Liu, X. Long, Z. Wei, Z. Wang, L. Zhang, J. Wang, F. Yan, S. Yang, *Angew. Chem. Int. Edit.* **2014**, *53*, 12571.

[35] X. Zheng, B. Chen, J. Dai, Y. Fang, Y. Bai, Y. Lin, H. Wei, Xiao C. Zeng, J. Huang, *Nat. Energy* **2017**, *2*, 17102.

[36] M. I. Saidaminov, J. Kim, A. Jain, R. Quintero-Bermudez, H. Tan, G. Long, F. Tan, A. Johnston, Y. Zhao, O. Voznyy, E. H. Sargent, *Nat. Energy* **2018**, *3*, 648.

[37] J. M. Ball, A. Petrozza, *Nat. Energy* **2016**, *1*, 16149.

[38] H. Uratani, K. Yamashita, *J. Phys. Chem. Lett.* **2017**, *8*, 742.

[39] W. Chen, K. Li, Y. Wang, X. Feng, Z. Liao, Q. Su, X. Lin, Z. He, *J. Phys. Chem. Lett.* **2017**, *8*, 591.

[40] D. Hong, Y. Zhou, S. Wan, X. Hu, D. Xie, Y. Tian, *ACS Photonics* **2018**, *5*, 2034.

[41] X. Wen, S. Huang, S. Chen, X. Deng, F. Huang, Y.-B. Cheng, M. Green, A. Ho-Baillie, *Adv. Mater. Interfaces* **2016**, *3*, 1600467.

[42] D. W. deQuilettes, W. Zhang, V. M. Burlakov, D. J. Graham, T. Leijtens, A. Osherov, V. Bulovic, H. J. Snaith, D. S. Ginger, S. D. Stranks, *Nat. Commun.* **2016**, *7*, 11683.

[43] J. Cao, S. X. Tao, P. A. Bobbert, C. P. Wong, N. Zhao, *Adv. Mater.* **2018**, *30*, 1707350.

[44] M. Stolterfoht, C. M. Wolff, J. A. Marquez, S. S. Zhang, C. J. Hages, D. Rothhardt, S. Albrecht, P. L. Burn, P. Meredith, T. Unold, D. Neher, *Nat. Energy* **2018**, *3*, 847.

[45] D. Luo, W. Yang, Z. Wang, A. Sadhanala, Q. Hu, R. Su, R. Shivanna, G. F. Trindade, J. F. Watts, Z. Xu, T. Liu, K. Chen, F. Ye, P. Wu, L. Zhao, J. Wu, Y. Tu, Y. Zhang, X. Yang, W. Zhang, R. H. Friend, Q. Gong, H. J. Snaith, R. Zhu, *Science* **2018**, *360*, 1442.

[46] W. Chen, Y. Zhou, L. Wang, Y. Wu, B. Tu, B. Yu, F. Liu, H. W. Tam, G. Wang, A. B. Djurisic, L. Huang, Z. He, *Adv. Mater.* **2018**, *30*, 1800515.

[47] Q. Wang, Y. Shao, Q. Dong, Z. Xiao, Y. Yuan, J. Huang, *Energy Environ. Sci.* **2014**, *7*, 2359.

[48] J.-W. Lee, D.-H. Kim, H.-S. Kim, S.-W. Seo, S. M. Cho, N.-G. Park, *Adv. Energy Mater.* **2015**, *5*, 1501310.

[49] W. A. Laban, L. Etgar, *Energy Environ. Sci.* **2013**, *6*, 3249.

[50] Z. Li, C. Zhang, Z. Shao, Y. Fan, R. Liu, L. Wang, S. Pang, *J. Mater. Chem. A* **2018**, *6*, 9397.

[51] D. Prochowicz, M. M. Tavakoli, A. Solanki, T. W. Goh, T. C. Sum, P. Yadav, *J. Mater. Chem. C* **2019**, *7*, 1273.

[52] N. H. Tiep, Z. Ku, H. J. Fan, *Adv. Energy Mater.* **2016**, *6*, 1501420.

[53] W. Chen, G.-n. Zhang, L.-m. Xu, R. Gu, Z.-h. Xu, H.-j. Wang, Z.-b. He, *Mater. Today Energy* **2016**, *1-2*, 1.

[54] Y. Zhou, F. Huang, Y.-B. Cheng, A. Gray-Weale, *Phys. Chem. Chem. Phys.* **2015**, *17*, 22604.